Durability of recycled fine mortars under freeze–thaw cycles

N. Algourdin, Q. N. A. Nguyen, Zyed Mesticou, Amir Si Larbi

Durability of recycled fine mortars under freeze–thaw cycles

N. Algourdin*, Q.N.A. Nguyen, Z. Mesticou, A. Si Larbi.

Université de Lyon, Laboratoire de Tribologie et Dynamique des Systèmes (LTDS), 58 rue Jean Parot, 42023 Ecole Nationale d'Ingénieurs de Saint-Etienne, France.

Corresponding author:

email: nonna.algourdin@enise.fr

phone: +33 (0)4 77 43 75 51

Abstract

The characterisation of recycled fine mortars under frost action was highlighted in this study. Mortars with three different ratios of recycled cement (RC), namely (10%, 30% and 50%) along with a reference mortar with 0% RC were prepared and subjected to freeze–thaw (F–T) cycles without air-entraining agents. After 96 F–T cycles, the specimens did not reveal any macroscopic damage; however, changes were noticed at a microscopic level. The pore diameter increased and the size of the rehydrated cement products decreased, especially in the case of 30% and 50% RC mixes. In this experimental study, the physical (mass loss and dimensional variation) and mechanical (flexural strength and dynamic elastic modulus) behaviour of the recycled mortar revealed that the critical period of structural degradation occurred during the first 24 F–T cycles.

Keywords

Recycled fine, Freeze–thaw weathering, Recycled mortars, MIP analysis, Mechanical properties

1. Introduction

Severe environmental impact from the cement industry is mostly caused by CO_2 emissions [1], which in turn, are caused by the production of clinker, which is a main key component in cement. Some studies have reported that cement manufacturing is responsible for 5%–7% of global CO_2 emissions [2]. One of the alternatives suggested for the reduction of emissions is 'waste valuing'. The use of recycled materials from demolished concrete reduces the systematic use of natural resources, especially in the case of recycled cement (RC) application. The RC powder is often included in cement-based mixes after different treatment processes, such as temperature application [3–7], carbonation [8,9] or filler integration [10]. Shui et al. [7] noted an increase in the compressive strength of recycled mortars, including fly ash, at temperatures between 300 and 800 °C, when preheated RC is included. Other authors [11,12] concluded that RC powder from demolished end-of-life concrete could re-cement under autoclave carbonation. Thus, the studies on RC properties have been scarce and need to be widened.

Being responsible for causing damage to ordinary and RC-based materials, frost can be a particularly important factor, especially when the freeze–thaw cycles alternate rapidly. Based on comprehensive experiments, it was concluded that the increase in the water content was not the main cause for the degradation of the cement-based materials; instead it is the pressure generated by the internal movement of water [13]. One of the theories is based on the concept of hydraulic pressure [14]. The moisture migrates from hot to cold areas under the influence of a thermal gradient. As ice constitutes the coldest area, the moisture moves to the ice crystals than condenses and turns into ice. The forces involved are so important that they cause local deformations and generate cracking. The second theory is based on osmotic pressure. Firstly, the water in the cement paste freezes in the large pores and then, in the smaller pores. The water in the interstitial phase of the cement-based material is not pure. Nevertheless, the freezing liquid attracts unfrozen water from small pores to restore the balance of concentrations by osmosis. These movements create so-called osmotic pressures [15]. On a material scale, numerous authors [16,17] have demonstrated that frost cementitious degradation is caused by a coupled thermo-hydro-mechanical phenomenon. The thermal contraction actions and cryosuction process induce a deterioration of the cementitious structure. Moreover, one of the important parameters that influence the frost resistance are the defects of microstructure, such as cracks and pits, as they maximize the contact between substrate and crystal [18].

According to some authors [19,20], the standardised frost tests in a water environment would not reproduce the real conditions for concrete structures and would be very severe for RC-based materials. In fact, the permanent level of sample water saturation keeps it covered with a waterproof foil, which prevents water evaporation, without being obstructed by free deformation. Moreover, in the

requirements laid out by the French Association of Civil Engineering (AFGC) [21] it is mentioned that concretes without salts having a water/cement (w/c) ratio greater than 0.5 are not resistant to frost. Moreover, a lot of authors [19,22–24] choose deliberately to make an exploratory study beyond the limits fixed by the standards.

Several authors have confirmed that the freezing and thawing resistance of recycled aggregate concretes is similar to that of normal aggregate concretes [25–28]. According to Liu et al. [29], considerable frost resistance can be obtained by using air-entrained recycled components or blending air-entrained and non-air entrained cement-based materials (with the latter being not less than 50% of the former). In addition, Gokce et al. [30] noted that non-air-entrained concrete was a serious handicap to achieve good freezing and thawing resistance, when used as recycled coarse aggregate in air-entrained concrete.

The frost resistance of mortars, including recycled powders, was investigated in this study because of a lack of availability of both credible scientific literature on this subject and a consensus on their properties after the F–T cycles. Thus, the aim of this study was to characterise the soaked RC-based materials under frost, immediately after the water curing, and before the internal drying. Firstly, the characterisation of the RC powder was performed by means of granulometry and absolute density. Secondly, three recycled mortars with substitution rates of 10%, 30%, and 50%, and one reference mortar (0% RC) were prepared. After 28 days of water curing, they were subjected to frost charge in an F–T machine under a constant relative humidity of 80%. The physical, microstructural, and mechanical properties before, during, and after the F–T cycles were discussed.

2. Experimental methodology

2.1 Characterisation of cements

The blast furnace cement CEM III/A 42.5 N-LH/SR CE PM NF was used as a reference. This type of cement is used in aggressive conditions, e.g., in situations involving contact with frost and de-icing salts in particular in road construction. By its content of blast furnace slag, it combines the advantageous characteristic of high tensile strength by splitting. Its low alkali content allows it to be used in combination with all traditional aggregates without the risk of reaction between the alkalis in the cement and the aggregates. The RC was extracted by electric sieving from a recycled sand of 0/2 mm size. The recycled sand was sourced from a demolished building and no additional information was available on the origin of the sand. The RC particle size was less than 80 µm. The RC was heated

at 500 °C and the cycle heating included a phase with a rise in the temperature (20 °C/min), a phase with a temperature dwell (3 h), and a cooling phase. The choice of particle size and its thermal treatment was based on previous experimental study [3]: SEM observation, TG/DTG/DSC thermal analysis and XRD analysis on oven-dried (80°C) and heated (500°C) RC were made. The RC at 80°C showed the presence of hydrated phases, as ettringite, which are dehydrated with the 500°C heating. It was concluded that the dehydrating method is efficient in increasing the RC reactivity. For the granulometry test, the RC was also oven-dried at 80°C until a constant mass was attained. This cement is referred to as RC 500 °C in subsequent discussion. After cooling, the RC was stored in plastic bags to limit air rehydration.

Two conventional experimental tests were conducted on the cement powder for physical characterisation, namely the density test and granulometry.

2.1.1 Density test

The absolute densities of CEM III/A 42.5 N and RC 500 °C cements were determined using a Le Chatelier pycnometer [31]. Firstly, the pycnometer was filled with a substance that is inert to the cement liquid (e.g., a solvent, such as white spirit). Next, 64 g of the cement was introduced carefully into the pycnometer using a mini-trowel. After the hermetic closure, all the elements were placed in a water bath at a constant temperature. The cement density was calculated as $\rho_{absolute} = \frac{m_c}{V_c}$, where m_c was the cement mass, and V_C was the cement volume. Each test was performed twice. The densities of the mortar components are shown in Table 1. The reference cement yielded a higher density than RC 500 °C.

Table 1 Densities of CEM III/A 42.5 and RC 500 °C cements

Cement type	**Density [kg.m^{-3}]**
Reference cement CEM III/A	2950
Recycled cement RC 500 °C	2668

2.1.2 Granulometry

The dispersion (grain size) of the reference and the RC was determined by OCCHIO500 nano XY image analyser (Figure 1) with CALLISTO 3D software, which performs a static image analysis. The dry cement sample is sprinkled onto the sample vessel, covering the aperture on the top of the cylindrical vacuum chamber. The bottom of the vacuum chamber is composed of a removable glass plate supporting the fine particles. The membrane vessel breaks down and the powder particles

disperse through the entire volume of the dispersion cylinder, when the vacuum reaches a critical level. The cement particles settle uniformly on the glass plate and the glass plate is moved automatically towards the imaging unit of the instrument. The digital video image reproduces the size and quantity of fine particles using a contrast between the particle and the background.

A statistical analysis package, integrated in CALLISTO 3D software presents the size of the particles, and calculates their quantity. Then, the fines are classified based on the largest size. One of the 200 photographs per measure is shown in Figure 2. The quantitative content of particles of different sizes was determined. The area equivalent dimeter with its mean values and mean intensity are given at the end of the measurements. In this study, three tests per cement type, with approximately 125,000 particles per measurement were performed.

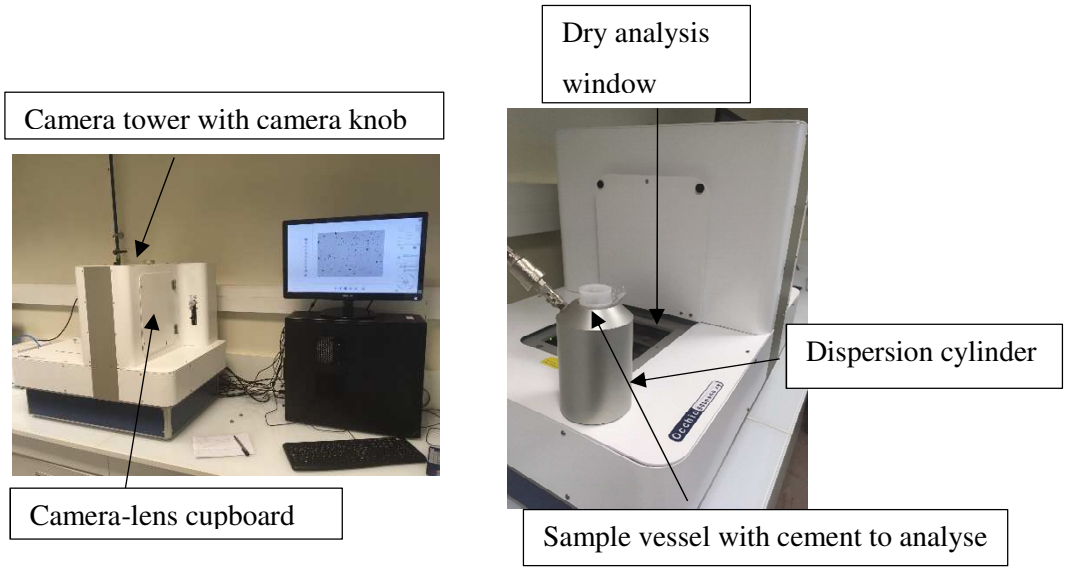

Figure 1 OCCHIO 500nano XY image analyser

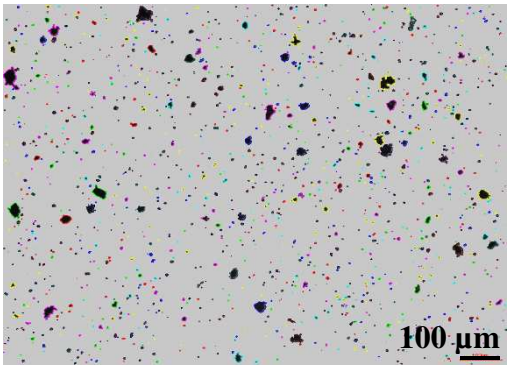

Figure 2 Example of particles taken from a dried sample with a resolution of 0.71 µm/pixel

Figure 3 presents the CEM III/A 42.5, RC 80 °C, and RC 500 °C cement area diameters as a function of the passing volume. The three curves follow the normal Gaussian distribution law. The CEM III/A

42.5 cement contained a finer fraction compared to the recycled cements from 10 to 95 µm area equivalent volumes. This was confirmed by the mean volume fractions, which were: $V_{CEM\ III/A\ 42,5}$ = 14 µm, $V_{RC\ 80\ °C}$ = 26 µm, and $V_{RC\ 500\ °C}$ = 20 µm.

The cement finesse is an important criterion for RC. In fact, the finer the RC, the fewer the pores and greater the mechanical resistance. The size distribution of RC 80 °C was shifted toward larger particles. This means that after heating, the volume fraction of the RC decreased. The difference was noticeable, especially for sieving diameters of 50 and 75 µm. As was shown by several authors [4,32], after 500 °C heating, the recycled cement powder was decomposed. The C-S-H gel, CH, and ettringite were replaced by non-crystalline dehydrated phases, and dehydrated C-S-H. The bound water loss led to the physical breakdown of the powder. Hence, RC heating was not only important from a chemical point of view [3], but also from a physical one.

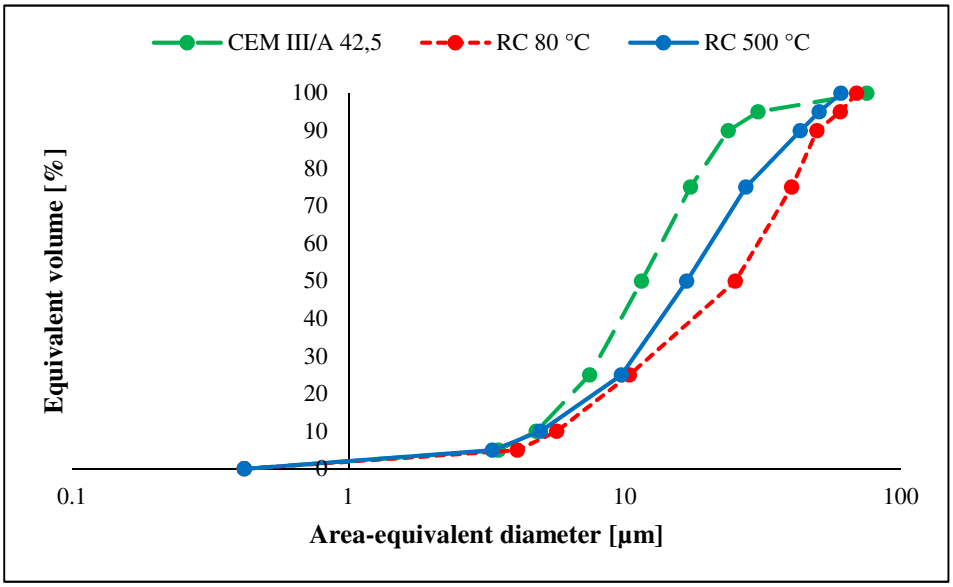

Figure 3 Non-cumulative particle size distribution of the cements

2.2 Mix design

The mortar mix proportions are listed in Table 2. The mortar workability is proportional to the ratio of the RC. The admixtures were not added to avoid a significant non-controlled effect during the freeze-thaw cycles with a risk of confusion of results and/or the interpretations. Standardised sand (SS) was used with a density of 2.64. according to the European standard NF EN 196-1 [33]. The w/c ratio of the mortar mixes was set to a high value (0.6), so as to favour frost degradation. 40 × 40 × 160 mm prismatic specimens were prepared according to NF EN 196-1. Next, 100 × 50 mm (height ×

diameter) cylindrical specimens were prepared for the dynamic elastic modulus test using a Pundit Lab instrument. The specimens were covered with polyethylene and kept in their moulds for the first 24 h, and then in water at a controlled temperature of 20 °C ± 1 °C until the 28-th day. Steel pins were integrated into three specimens per mix for shrinkage measurements.

Table 2 Mix proportions of mortars

Mortars	**Mixture proportions [kg.m^{-3}]**			
	CEM III/A 42.5 cement	**Recycled cement**	**Sand**	**Water**
0% RC	300	0	1909	180
10% RC	272	27	1909	179
30% RC	229	61	1909	178
50% RC	197	99	1909	179

2.3 Freezing–thawing cycles and monitoring

The mortars were placed in a freezing–thawing machine (Fitoclima 300), designed for a strict and precise control of the environmental conditions with a volume of 300 L (Figure 4 a). Type K thermocouples were positioned inside the machine, at the centre of the prismatic specimens to monitor the temperatures (Figure 4 b).

A testing procedure close to the one prescribed by Rilem recommendations TC 176-IDC [34] was adopted. During the freeze–thaw cycles, the specimens were stored in air with a constant relative humidity (RH) of 80%. Each tray was covered with a plastic film to avoid excessive evaporation. The temperature cycle varied from 19.8 to –19.9 °C in the freezing–thawing machine and from 18.3 to –18.8 °C in the centre of the specimen, as shown in Figure 5. The duration parameter was, however, modified. One F–T cycle lasted 7 h. Small temperature variations (T_{air}) were observed owing to the temporary opening of the machine to take out the specimens for the weekly tests.

The specimens were examined and tested every seven days. A total of 96 cycles were performed over 28 days.

(a)

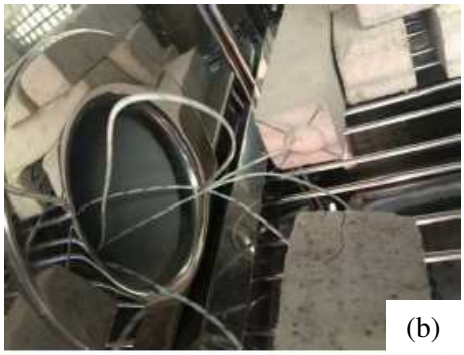

(b)

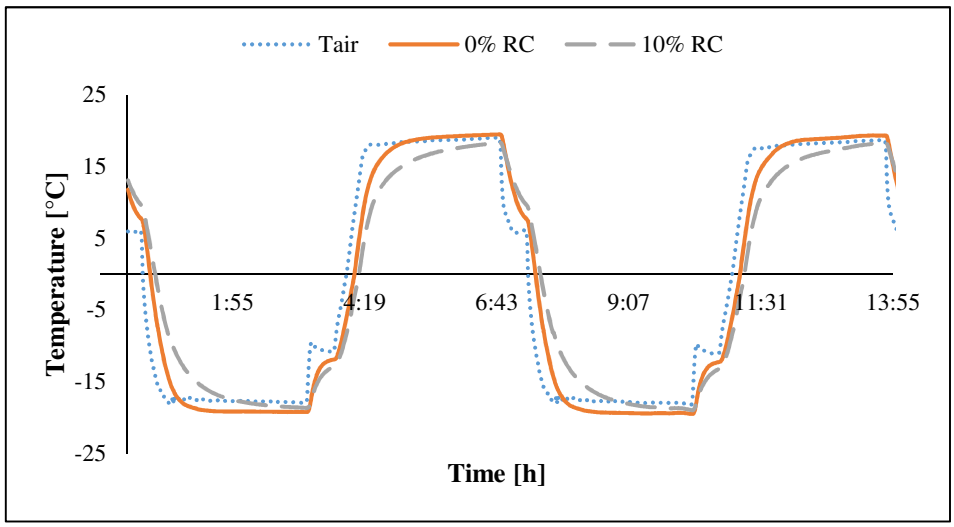

Figure 5 Real cycle of freezing-thawing test. T_{air} – temperature inside the F-T machine

2.4 Test methods

The evolution of the concrete microstructure was studied using scanning electron microscopy (SEM), water porosity, and mercury intrusion porosity (MIP). The physical mortar properties were investigated through density, loss of mass, and drying shrinkage. Compressive (f_c) and flexural strengths (f_t), and dynamic modulus of elasticity (E_{dyn}) were measured to estimate the mechanical degradation of the samples.

Scanning electron microscopy analysis: Two samples of each mortar were collected after the mechanical tests, dried at 80 °C, and metallised with gold. Tests were performed using a TESCAN Vega microscope with a high vacuum chamber of 10^{-2} Pa pressure.

Water-accessible porosity (P_{tot}): Three samples per mix were placed in a vacuum cell for air extraction and water filling. The 40 × 40 × 80 mm samples were dried at 80 °C until a constant mass was attained before the test.

Mercury intrusion porosity: Two samples for each mix were dried at 80 °C and tested on Micrometrics Autopore IV. Various levels of pressure were applied from 3×10^{-3} to 200 MPa, covering a pore diameter range of 0.003–370 µm.

Mass loss: The mortar mass loss was determined every 7th day from the 28th day. Three samples per mix were used for mass loss monitoring.

Drying shrinkage: The dimensional variation of the 40 × 40 × 160 mm mortar specimens was made according to the European standard NF P15-433 [35]. The test was conducted on three specimens per mix.

Compressive (f_c) and flexural (f_t) strengths: Three 40 × 40 × 160 mm^3 specimens per mix were tested. Firstly, the specimens were placed in a hydraulic press for flexural strength, and a vertical load was applied on the lateral side of the prism until rupture, following the procedures described in the European standard NF EN 196-1 [33]. Secondly, compressive loading with an imposed stress rate of 2400 N/s was applied to the two halves of the broken prisms after the flexural test was performed.

Dynamic modulus of elasticity (E_{dyn}): A wave propagation test device from Pundit Lab was used for the P-wave velocity (V_p) measurement. Knowing the velocity (V_p) and Poisson's ratio (ν = 0.2), it is possible to calculate the value of E_{dyn} (Eq. 1). The dry apparent densities (ρ) were measured by hydrostatic weighting during the total porosity tests according to NF P 18-459 [36].

$$E_{dyn} = \rho V_p^2 \frac{(1+\nu)(1-2\nu)}{(1-\nu)} \quad (1)$$

3. Results and discussions

During the 28 days of freezing-thawing tests, there was no spalling or cracking damage observed to the naked eye in any of the specimens.

3.1 Microstructural analysis

3.1.1 SEM analysis

Figure 6 shows the SEM images of the 0% (a) and 50% RC (b) mortars. Some microcracks were observed in the 50% RC sample. The employed w/c ratio was relatively high (0.6) because of the high water demand of the RC mixes. The increase in the volume of the frozen water was approximately 9%. Thus, excessive water was entrapped in the voids during the F–T cycles, which generated forces into the materials that led to the cracks. Figure 7 (a) presents a foil-like C-S-H gel on the 10% RC specimen and numerous ettringite needles on the 30% RC mortar (Figure 7 (b)). A structural modification of the ettringite needles was observed between 0 and 96 F–T cycles (Figure 7 and Figure

8). The ettringite acted as a fibre modification and CH did not present a typical hexagonal shape. This was confirmed by the denser microstructure and lower porosity of the reference mortar [7]. Moreover, it was observed that the sizes of the rehydrated cement products, such as C-S-H gel and calcite were smaller than that of the reference cement product.

Some authors [37,38] remarked that the hydrate elements as C-S-H were intact after the F–T cycles. After the quantitative image analysis, it appeared that the number and volume repartition of the hydrates did not change after the F–T cycles in this study.

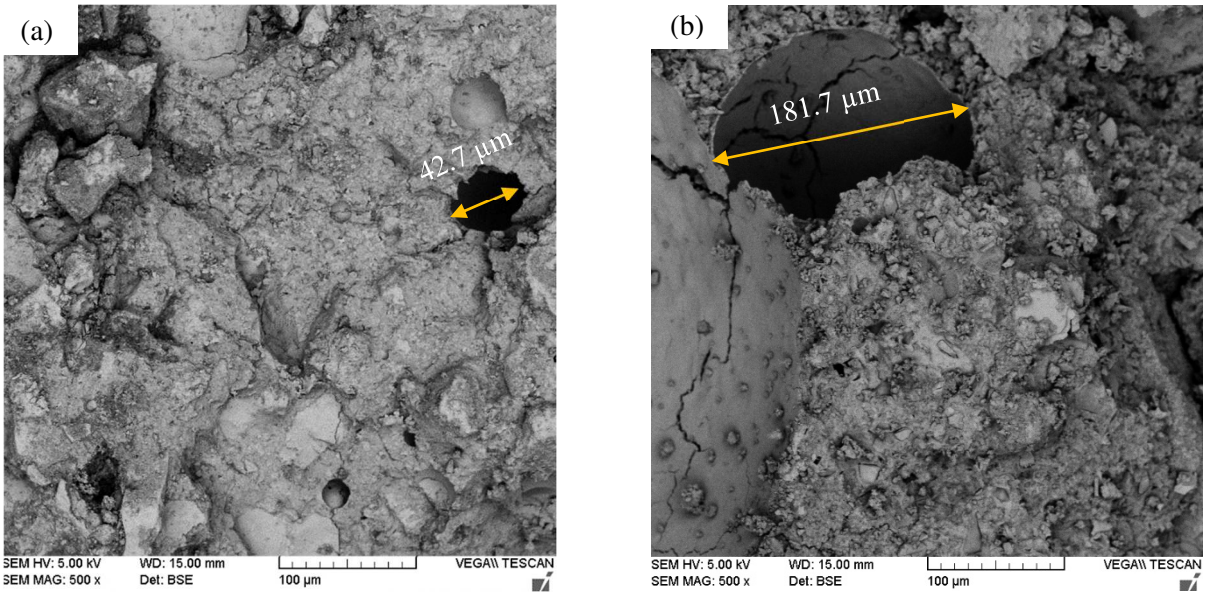

Figure 6 SEM images of (a) 0% RC and (b) 50% RC mortars after 96 F–T cycles

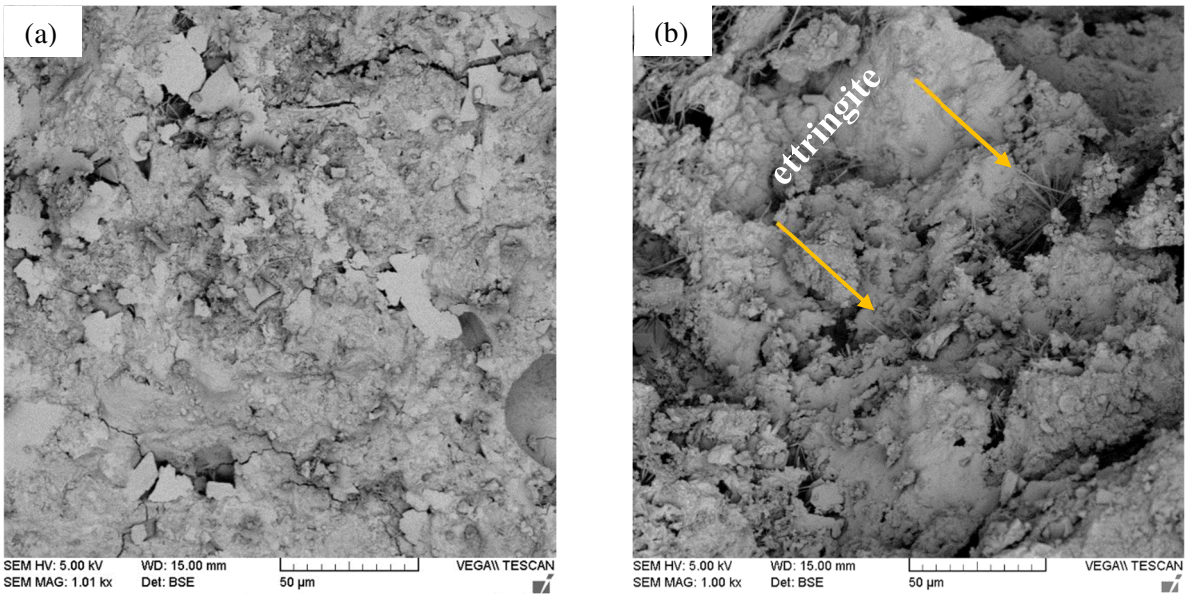

Figure 7 SEM images of 10% RC (a) and 30% RC (b) mortars before F–T cycles

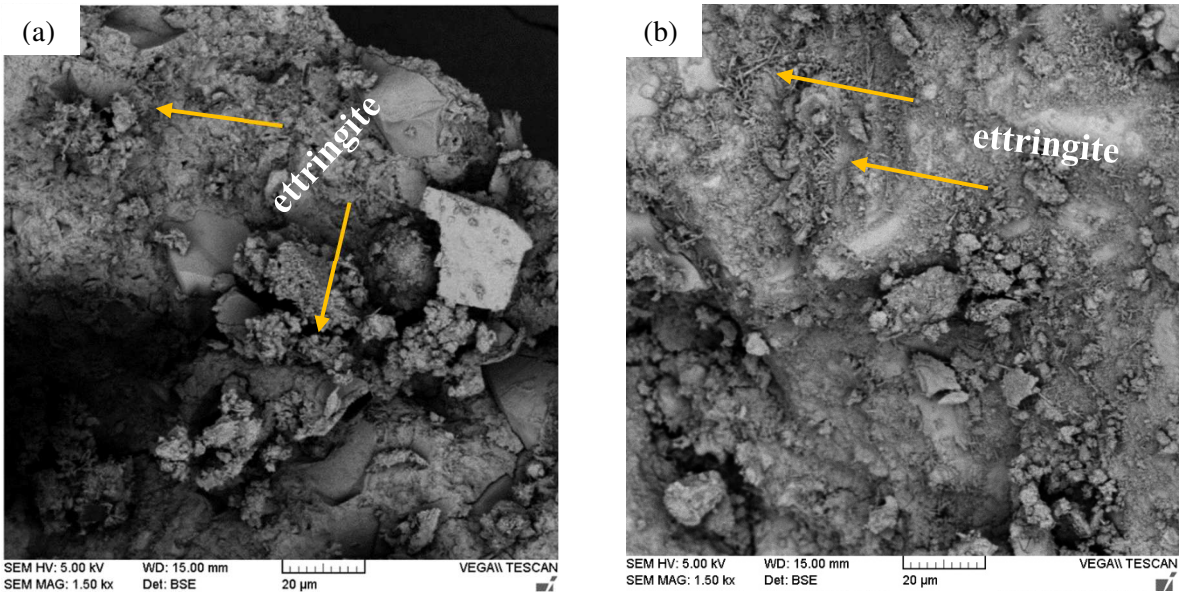

Figure 8 SEM images of 0% RC (a) and 30% RC (b) mortars after F–T cycles

3.1.2 Porosity

Figure 9 presents the water and mercury porosity evolutions as a function of the F–T cycles. The water-accessible porosity of all the mortars increased slightly with the number of the F–T cycles. The minimum and maximum values were: $P_{tot\ min\ 30\%\ RC}$ = 22.8% to $P_{tot\ max\ 50\%\ RC}$ = 26.8%. The most important water porosity increase of 0.83 % occurred between 72 and 96 F–T cycles for the 50% RC mortar, confirming the presence of an internal crack network (SEM observations (Figure 6)). The water porosity evolution of the 0% and 10% RC mortars had a close progress up to 72 F–T cycles, and the porosity of the 0% RC mortar became more significant, which matched the results for the loss of mass.

The mercury porosity was measured at 0 and after 96 F–T cycles. The values of the mercury porosity were lower for all the mortars, except for the 0% RC mix, compared to the water porosity. This finding was also recorded by several authors [39]. During the mercury porosity test, only the pores ranging from 0.003 to 370 µm were filled, while prior studies without kinetics mention that all the pore dimensions are accessible for water. Thus, mercury intrusion measurements underestimate the volume of large pores [40]. In addition, the large volume of pores related to the hydrate calcium

silicates C-S-H was only partially accessible for this measurement technique. For cementitious materials that present both low capillary porosity and large C-S-H quantity, the proportion of non-accessible pores increased. This showed the difference between the two measurement techniques, which resulted in a difference between the recorded values.

According to Omary et al. [41], the porosity of the concrete depends strongly on the total porosity of the cement paste that sticks the particles together. The maximum difference in the water porosities between the reference and recycled cement mortar was less than 1.3% and could not considerably reduce the adherence capacity of the aggregates

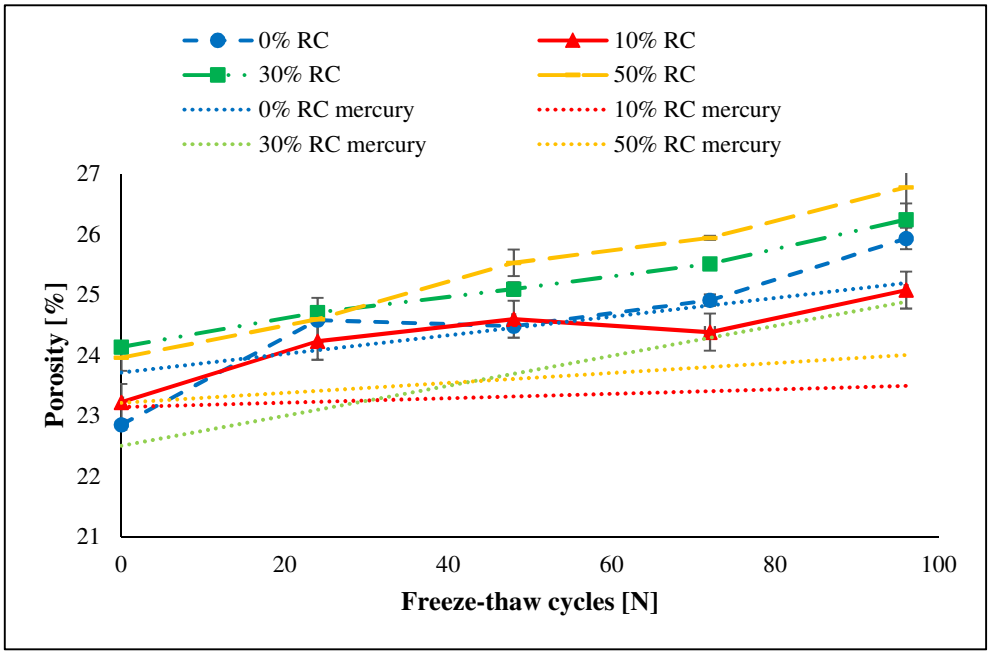

Figure 9 Evolution of water and mercury porosity of mortar mixes versus number of F–T cycles. [N] – number of freezing-thawing cycles.

The mercury porosity allows for the determination of the mortar pore distribution, as well as the morphology. Figure 10 presents the differential pore size distribution of the mortars at 0 and after 96 F–T cycles. The minimum and maximum pore distributions corresponded to the measuring capacity of the device. It is possible that the mortar contained more pores below or above the measured range. All the mixes presented a heterogeneous porous network.

According to Walbert [42], three pore classes exist, namely microporous (pore diameter < 1 µm), mesoporous (pore diameter from 1 to 10 µm), and macroporous (pore diameter > 10 µm). For all the mortars, the majority of pores were located in the microporous regime; specifically, 0% RC – 80%, 10% RC – 87%, 30% RC – 77%, and 50% RC – 72%, at 0 F–T cycles. After 96 F–T cycles, a slight

transformation of the micropores to mesopores was noticed for the 0% RC mortar. The micropore number decreased from 80% to 75%. Tenoutasse et al. [43] compared the mortar cracking sensitivity to its mesopore rate (between 0.57 and 0.11 µm); that is, the greater the pore range, the lower the durability. After a frost action, the quantity of macropores increased slowly as follows: for 0% RC – 5%, for 10% RC – 3%, and for 30% RC – 7%, while for the 50% RC mix, the proportion of micropores was 17%. This non-significant increase was owing to the connection of the capillary pores by microcracking. Jacobsen et al. [44] noted that the frost action would induce a rise in the total porosity by increasing both the ratio of the small pores, which were below the inflexion point of the mercury intrusion curve, and the ratio of the large pores (> 1 µm). Before the frost action, the peaks were present in mesoporous and macroporous zones, i.e., at 4.7, 13.9, and 26.9 µm for the 50% RC mortar. After 96 F–T cycles, this pore percentage increased in this area and presented two remarkable peaks at 15.42 and 32.3 µm. After the 96 F–T cycles, the pore diameter increased significantly for the 30% RC and 50% RC mortars; consequently, these formulations were more likely to be affected by the freeze damage. According to some authors [45,46], the solidification temperature of the interstitial solution depended mainly on the pore size, in which it was confined; therefore, the freeze damage increased with a high proportion of large and connected pores.

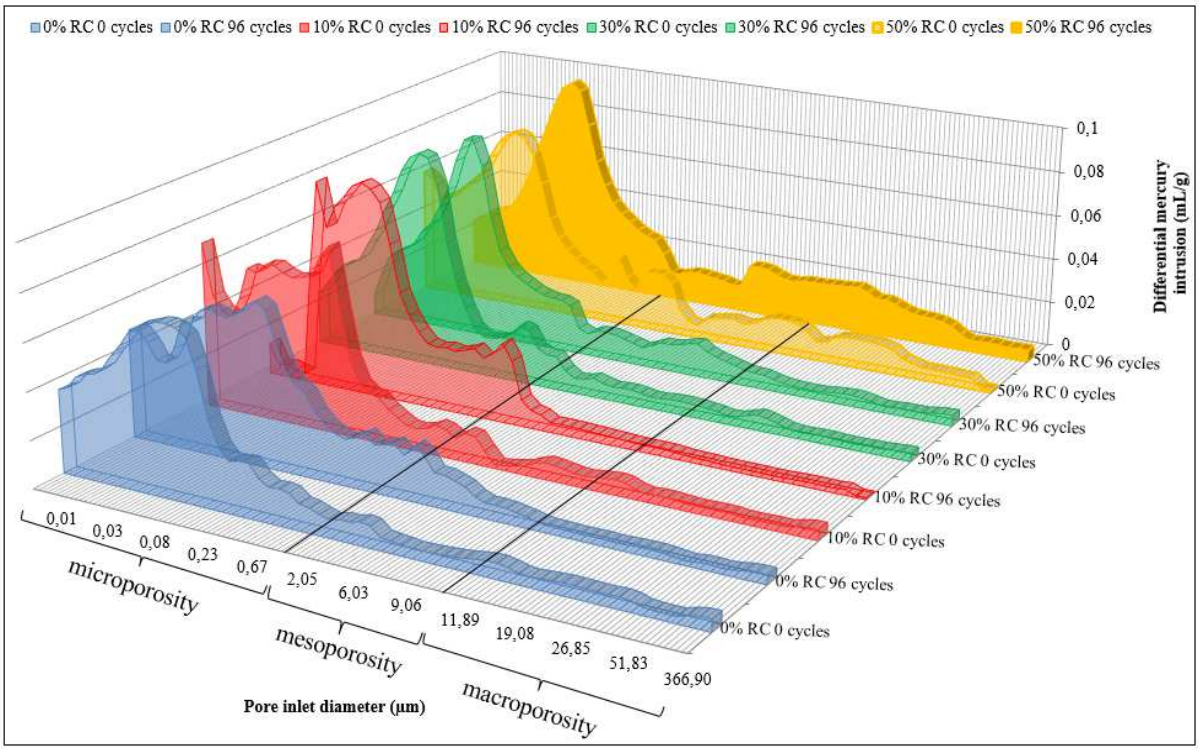

Figure 10 Differential pore size distribution of mortars at 0 and after 96 F–T cycles

Fractions for gel (d < 0.01 µm) and capillary pores (d > 0.01 µm) [47] of tested mortars are presented in Table 3. The pore evolution was different for reference (0% RC) and recycled mortars (10% RC,

30% RC and 50% RC): after 96 F-T cycles, the 0% RC mortar showed pore increase in the same fraction, while the two recycled mortar fractions decreased. For recycled mortars, the average decrease of gel pores was by 6.7% and for capillary pores by 9.9%. F-T cycles modified the microstructure of recycled mortars by decreasing the quantity of small pores and passing to larger capillary pores.

Table 3 Percentage of pores by pore category

Type of mortar	**Pore percentage %**	
	Gel pores (d < 0.01 µm)	**Capillary pores (0.01 µm < d < 0.05 µm)**
0% RC 0 cycles	6.6	33.4
0% RC 96 cycles	7.0	36.1
10% RC 0 cycles	10.2	42.0
10% RC 96 cycles	2.0	27.4
30% RC 0 cycles	5.9	38.6
30% RC 96 cycles	3.1	26.5
50% RC 0 cycles	4.1	34.1
50% RC 96 cycles	3.2	31.2

Figure 11 presents the median diameter (d_{50}) of the porous network at 0 and after 96 F–T cycles. The median diameter corresponded to 50% of the cumulative intrusion curve in percentage and pore diameter in µm. The median diameters of the RC samples were similar to that of the reference before the frost effect and increased after 96 F–T cycles because of the mortar internal damage. The average increase in the median diameter for the recycled mortars was 0.03 µm. The reference mortar had the largest median diameter of 0.08 µm; nevertheless, it did not change after the frost action.

The free and trapped porosities characterise the percentage of porosity based on its behaviour with regard to the wetting fluids. The free porosity becomes saturated with a wetting fluid and is completely restored during the desaturation of the milieu. The trapped porosity has a different behaviour because it does not become saturated with the fluid during the mercury fill procedure; nor does it release the fluids during the drainage [48]. Figure 12 presents the percentage of trapped porosity of mortars at 0 and after 96 F–T cycles. The trapped porosity was higher after the freeze–thaw action for all the mortars, with the exception of the 10% RC mix. The increase in the trapped porosity could be owing to the internal network damage. A high percentage of trapped porosity could also indicate that the pores were poorly connected. The pore network contained macropores with small capillary pore connections.

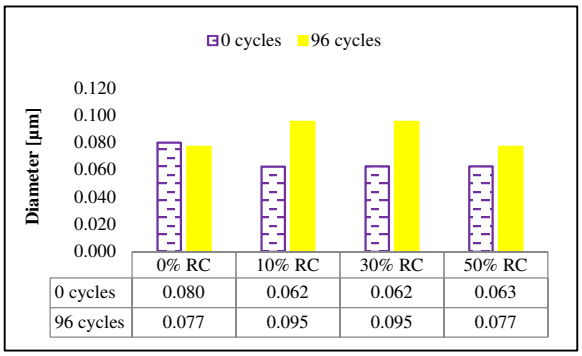

	0% RC	10% RC	30% RC	50% RC
0 cycles	0.080	0.062	0.062	0.063
96 cycles	0.077	0.095	0.095	0.077

Figure 11 Median diameter (d_{50}) of mortars before the first F–T cycle and after 96 F–T cycles

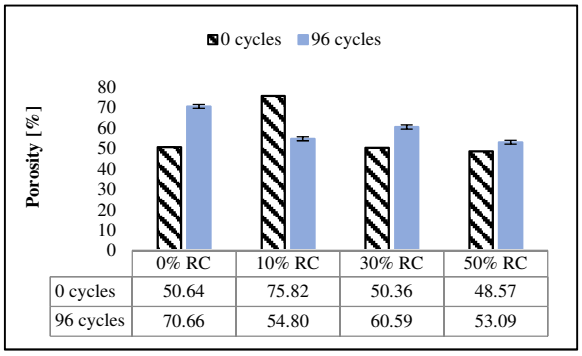

	0% RC	10% RC	30% RC	50% RC
0 cycles	50.64	75.82	50.36	48.57
96 cycles	70.66	54.80	60.59	53.09

Figure 12 Trapped porosity of mortars before the first F–T cycle and after 96 F–T cycles

3.2 Physical properties

3.2.1 Apparent density and mass loss

The apparent density evolution is shown in Figure 13. The density decreased with the number of F-T cycles. Between 0 and 24 cycles, a significant decrease in the density was observed with an average loss of 2.3%. This decrease could be linked to the mortar drying after water conservation, and was consistent with the evolution of the mass loss. After 48 cycles, the density loss was relatively inconspicuous and minimal for all the mixes compared to the 0% RC mortar, i.e., the reference. Except for the drying processes owing to the RH change from 100% to 80%, the density of the mortars did not change significantly during the freeze–thaw cycles, as was observed in the study of Zhang et al. [49].

There was no significant difference in density evolution between the 0% and 10% RC mortars. Moreover, the 0% and 10% RC formulations lost more density (3.6%) than the 30% and 50% RC mortars (2.7%) before the beginning of the F–T cycles and after 96 F–T cycles. The 50% RC mix presented the lowest density during the F–T cycles. The total porosity (Figure 9) and SEM (Figure 6) results confirm the presence of a larger porous network for this mortar.

The mass loss values for all the samples are shown in Figure 14. The mass loss decreased with the number of F-T cycles. The highest mass loss of all the mortars was observed after 24 cycles, with an average value of 3.06%. Wang et al. [42] noted that during the F–T cycles, the excessive mass loss rate (> 5%) could present the beginning of the feebleness of the cement-based material. In this study, the specimens did not show degradation; nor did they present an excessive mass loss (> 5%). The

significant mass loss at the beginning of the F–T cycles was owing to the HR difference; the specimens were dried from 100% (curing) to 80%. After 48 F–T cycles, the 0% RC mix showed an insignificant mass loss compared to the RC mortars. This could be explained by its smaller porous network, as revealed by the mercury porosity that it soaked less water during the curing period. For all the F–T periods, the 50% RC showed the highest mass loss. This was consistent with the lowest density of this mortar (Figure 13) and the trapped porosity results. The 50% RC trapped porosity presented lower values; therefore, the free porosity allowed water to drain away more easily.

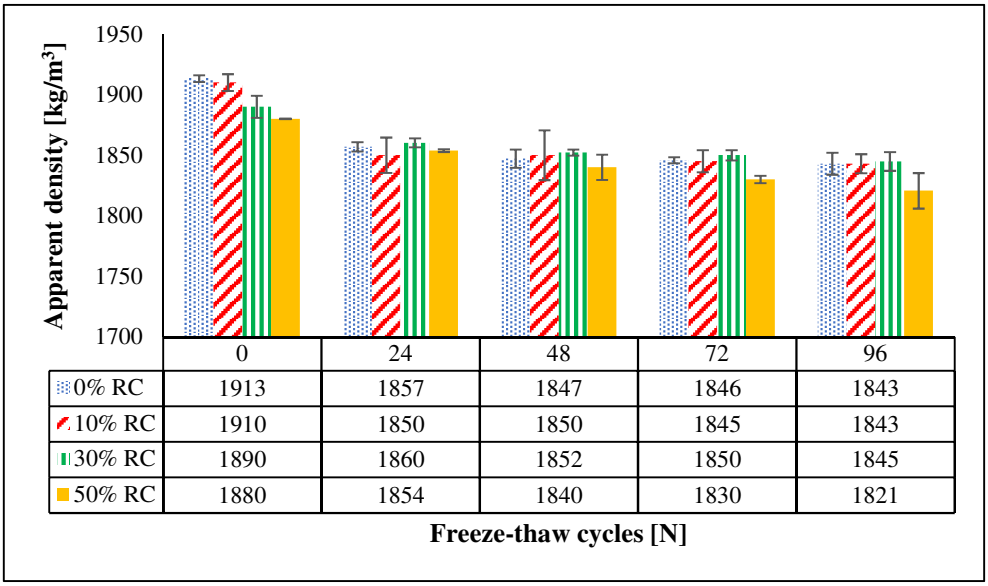

	0	24	48	72	96
0% RC	1913	1857	1847	1846	1843
10% RC	1910	1850	1850	1845	1843
30% RC	1890	1860	1852	1850	1845
50% RC	1880	1854	1840	1830	1821

Figure 13 Apparent density versus number of F–T cycles

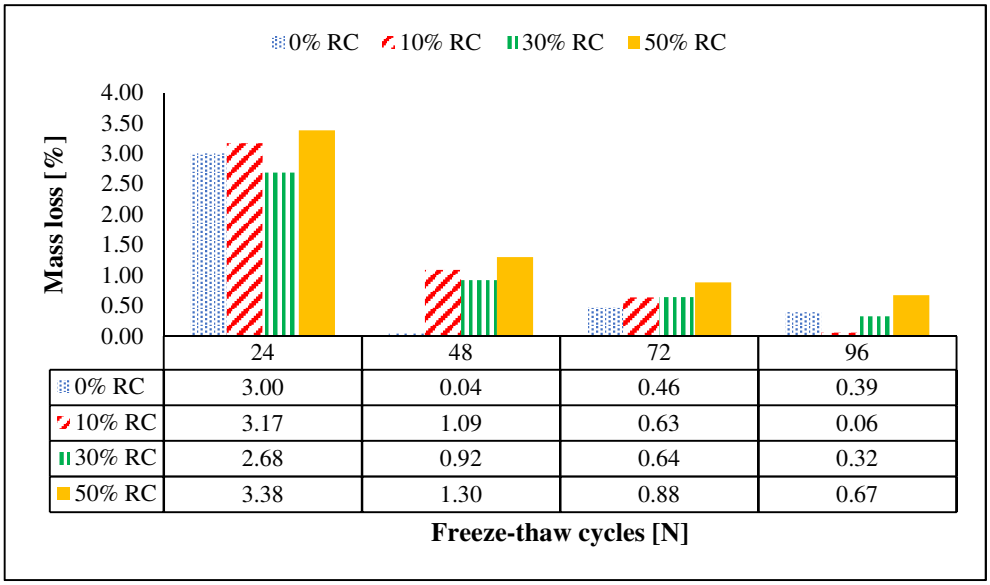

	24	48	72	96
0% RC	3.00	0.04	0.46	0.39
10% RC	3.17	1.09	0.63	0.06
30% RC	2.68	0.92	0.64	0.32
50% RC	3.38	1.30	0.88	0.67

Figure 14 Mass loss versus number of F–T cycles

3.2.2 Dimensional variation

The dimensional variation test results are plotted in Figure 15. The standard deviation values were too small to be visible on the graph. All the mix-designs exhibited drying shrinkage during the F–T cycles. Between 24 and 96 F–T cycles, the specimen's drying shrinkage presented a descendent evolution. The highest dimensional variation was observed between 0 and 24 cycles (relative average length = 0.09%). At the start of the F-T cycles, the specimens were on the top saturation and, for this reason, presented a more important shortening. In these experimental conditions, the period between 0 and 24 cycles appeared to be critical for specimens, resulting in possible degradation. The results showed that the obtained maximum shrinkage was not sufficient to cause cracking or breaking off of the mortar specimens.

The 0% RC showed less shrinkage than the RC mortars. As was shown by Algourdin et al. [36], the dehydrated RC needed more water than the reference cement. The smaller quantity of soaked water induced a smaller deformation. The dimensional variations of 10% and 30% RC mix-designs had a very close evolution during the frost test. The negative lengthening indicates not only a thermal expansion, but also water shrinkage, related to the migratory water desorption from the gel C-S-H hydrate pores.

The 0% RC mortar shrinkage after 96 F–T cycles almost reached the initial value. The descendent shrinkage evolution could indicate the premature beginning of the extended drying phase. Moreover, the mercury porosity study highlighted the increase in the pore size after 96 F–T cycles between 6 and

300 µm, especially for the 30% and 50% RC mortars, which ensured an easier water migration and evaporation.

The results of the drying shrinkage corroborate the mass loss evolution. Generally, three phases were observed. The first was characterised by a significant mass loss with a slight shrinkage; in the second phase, the shrinkage increased considerably as a function of the mass loss; and the third phase resulted in a clear decrease in the shrinkage associated with the stabilisation of the mass loss [50]. In this study, the first phase presented the highest shrinkage associated with the highest mass loss. This was owing to the change in the curing conditions (HR 100% → 80%).

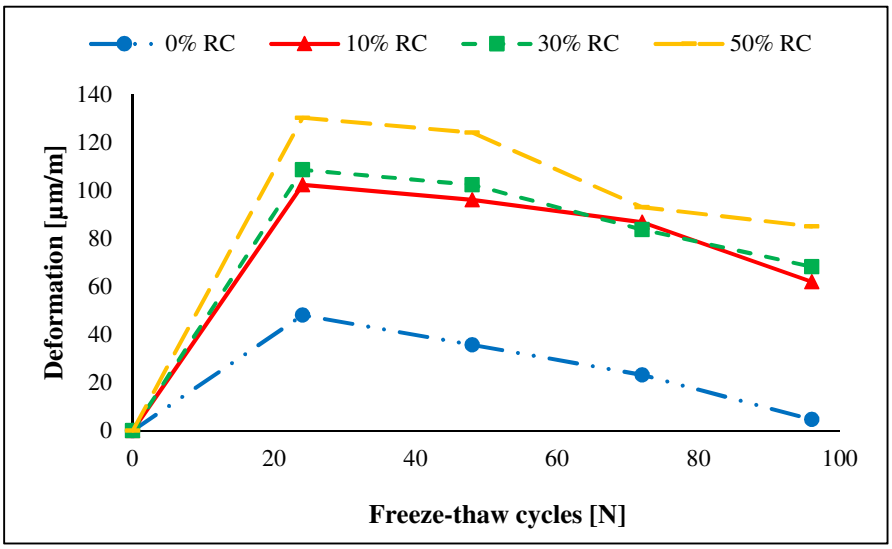

Figure 15 Mortar shrinkage with different amounts of RC versus number of F–T cycles

3.3 Mechanical properties

3.3.1 Compressive strength

Figure 16 depicts the compressive strength (f_c) as a function of the F-T cycles. The 0% and 10% RC formulations presented the highest f_c throughout the F–T cycles, and the 50% RC mix showed the lowest f_c. Between 0 and 24 cycles, f_c showed a slight descending evolution. The maximum difference was a loss of 1.54 MPa for the 50% RC mix. After 24 F–T cycles, the f_c values of the 0% and 30% RC mortars increased with a maximum gain between 24 and 96 F–T cycles of 2.3 MPa for the 30% RC mix. It should be noted that the reference cement had a low hydration heat; thus, its resistance increase could last longer and the trend of the curve confirmed the same. The 10% and 50% RC presented an f_c rise between 24 and 72 F–T cycles and then a rise in the slope. Xiao et al. [51] remarked that f_c of the RC-based materials was lower than that of Portland cement mixes. The main reason for this is that the

RCs have high water absorption. Nevertheless, it may be supposed that owing to the higher water content, the RC matrix continued to hydrate significantly after 28 days of curing, which caused a significant increase in f_c during the F–T cycles, more so for the 50% RC mix. Yildrim et al. [52] studied the saturation influence of nine RCs with w/c ratios of 0.5, 0.6, and 0.7 under frost action. Before the F–T cycles, the saturation concrete degrees were 0%, 50%, and 100%. It was concluded that the complete and 50% saturation samples enhanced the F–T mechanical resistance of the concretes. This increase was probably, owing to the additional cement matrix hydration.

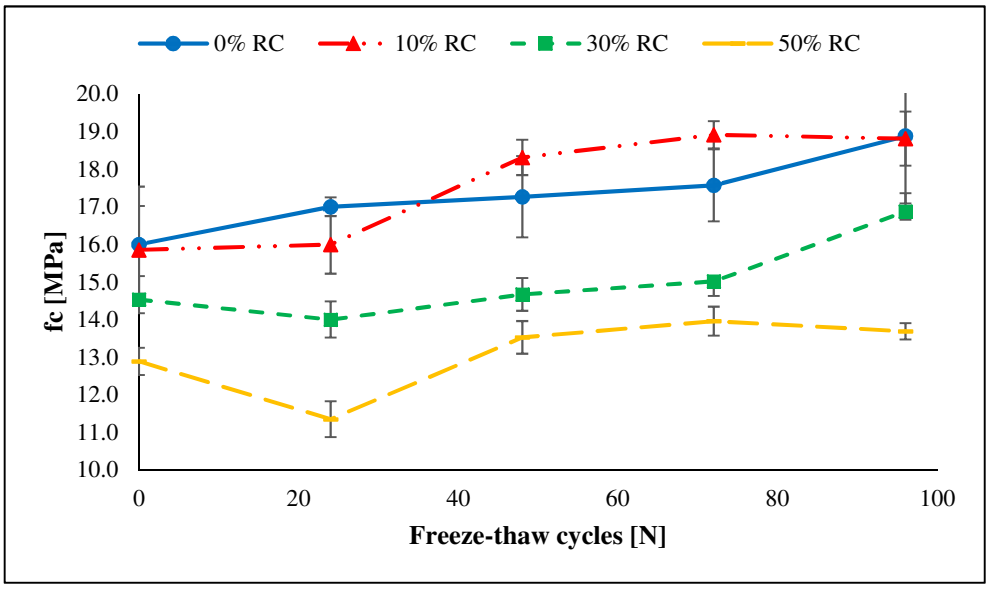

Figure 16 Evolution of f_c of mortar mixes versus number of F–T cycles

3.3.2 Flexural tensile strength

The evolution of flexural tensile strength (f_t) as a function of F-T cycles is presented in Figure 17. An important f_t drop was observed between 0 and 24 F–T cycles for all the mortars. The dimensional variation results (3.2.2) indicated a considerable drying shrinkage at the beginning of the freezing action, which could generate significant crack network, especially on the surface of the specimens. Thus, f_t was possibly affected by the surface crack network development and the porosity increase (Figure 9). After 24 F–T cycles, the f_t evolution was primarily constant for the 10% and 30% RC mortars. The 0% and 50% RC mixes had a variable evolution, marked by slight rises and descents. As in the case of Eslami et al. [51], it was difficult to analyse and predict the f_t evolution for these two mortars.

Prosek et al. [53] tested 21 RC mortars with replacement amounts ranging from 10% to 50% and a water/binder ratio of 0.35. It was noted that the presence of the RC had a reinforcing effect on the

flexural tensile strength. The same trend was observed in this study, but less marked under the frost action.

f_t had a more marked decrease than f_c. f_t was significantly influenced by the cement matrix/aggregate interaction state, while f_c was mostly governed by the sliding and crystal arrangement. As the internal gel first attacked the cement matrix/aggregate zone [54], f_t showed more damage. f_c could be more or less sensitive to the microstructure damage depending on the direction of microcracks and their spatial distribution. If the damage was superficial and the cracks were mainly located on the surface, f_c could be less affected by the presence of cracks. Furthermore, the compression test close microcracks, while during flexural test, the microcracks open and propagate more easily.

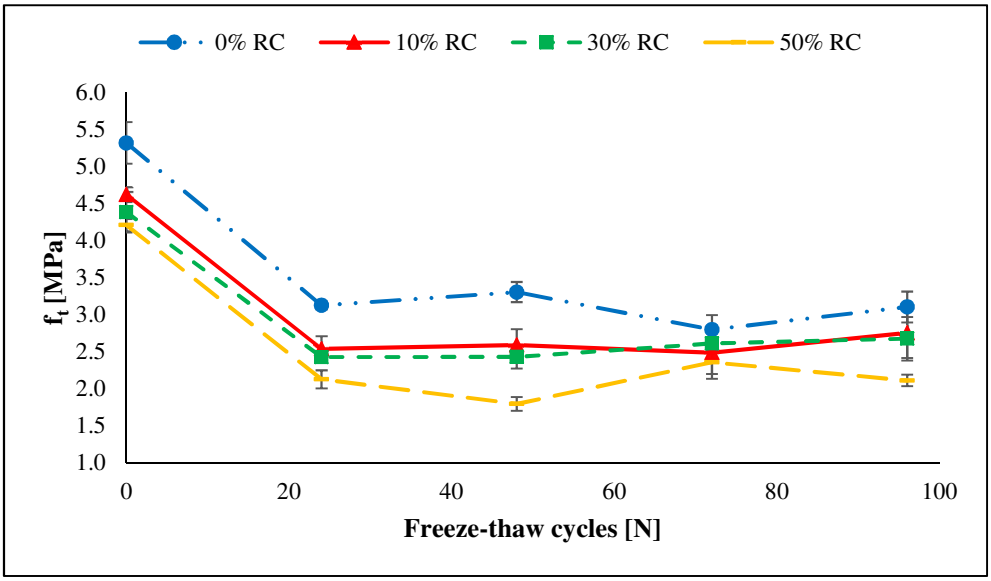

Figure 17 Evolution of f_t of mortar mixes versus number of F–T cycles

3.3.3 Dynamic elastic modulus

Figure 18 presents the E_{dyn} evolution as a function of the F–T cycles. Similar to f_t, E_{dyn} exhibited a descendent evolution between 0 and 24 cycles, which indicated the growth and propagation of cracks. After 24 F–T cycles, all the mortars showed a slight rise up to 96 F–T cycles. This evolution corroborated the f_c results and confirmed that the cement paste was under continuous hydration. The 0% RC mortar showed the highest E_{dyn}. The 30 % and 50 % RC mixes showed a similar evolution, except between 72 and 96 F–T cycles. In fact, E_{dyn} of 50% RC mortar showed a low descending evolution that was in accordance with the f_c and f_t results. Zaharieva et al. [19] tested three types of recycled concretes, namely with recycled coarse aggregates, with 100% water pre-soaked recycled aggregates, and with 100% non-pre-soaked recycled aggregates) by applying a protocol close to NF P

18-424 [55]. E_{dyn} did not present a significant decrease. The author's results were distinct from those of our study. The difference in the F–T test programs appeared to be a crucial for the evolution of the mechanical characteristics.

Liu et al. [29] conducted E_{dyn} tests on non-air-entrained and air-entrained specimens over 250 F–T cycles. The results demonstrated a slight decrease in E_{dyn} for mixes containing recycled materials, derived from a high-strength parent concrete, and a high decrease for concretes containing ordinary recycled concrete. It appears that the original concrete type played an important role in the mechanical characteristics of RC-based materials.

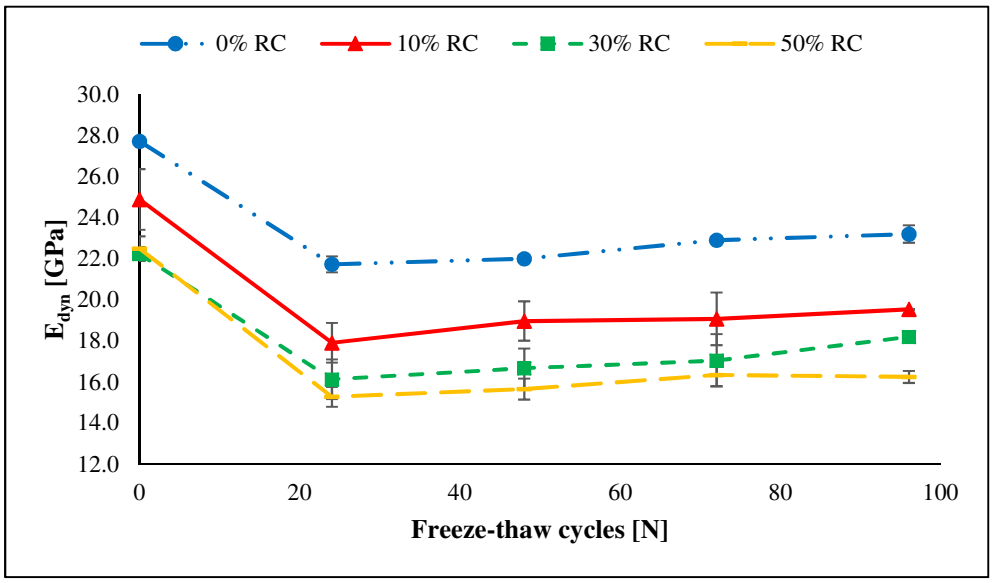

Figure 18 E_{dyn} evolution of mortars versus number of F–T cycles

4. Conclusions

Considering the significantly diverse results available in the literature, an exploratory experimental F–T program was conducted on one reference (0% RC) and three recycled mortar formulations with substitution levels of 10%, 30%, and 50%. The density and granulometric characteristics of the recycled powders were determined for further preparation of recycled mortar formulations. The recycled mortars were characterised before and during the F–T cycles. The assessed critical F-T parameters, as water and mercury intrusion porosity were completed with the contributing parameters, as dimensional variations, mass loss and mechanical strength. The following conclusions were drawn from the test results reported herein:

- The particle size distribution was lower for RC at 500°C, than that of RC at 80°C. This was owing to the chemical decomposition of the C-S-H gel and ettringite.
- Significant evolution of physical properties during the first 24 F-T cycles was noted for all the mortars. The 50% RC mortar presented the lowest density and the highest mass loss, which was in accordance with the SEM and MIP analyses, namely the presence of a larger porous network. Changes in the environmental conditions (HR 100% – 80%) were the most significant influencing factors.
- The design of three recycled and one reference mortars with w/c of 0.6 did not show any macroscopic damage after 96 F–T cycles. The trends are valid for this type of mortars. On a microstructural level, the microcracking of capillary pores was noted. SEM observations and MIP analysis showed decrease of small gel and capillary pores of all recycled mortars (10% RC, 30% RC and 50% RC).
- The increase in the pore diameter for 30% and 50% RC compositions was also confirmed through SEM observations and MIP analysis.
- The mechanical characteristics (f_t and E_{dyn}) decreased slightly between 0 and 24 F–T cycles, which was in accordance with the water porosity test, and its overall evolution is positive. Basing also on the drying shrinkage results, the structural instability period for the recycled mortars occurred between 0 and 24 F–T cycles, and after passing this period, the physical and mechanical specimen properties did not change significantly.

In summary, this study presented our experimental findings on the frost resistance of recycled mortars, but under a single frost action. Further work can be undertaken to study the damage and deterioration of recycled mortars or concretes subjected to coupled thermomechanical action. Moreover, a longer F–T cycle period should be tested to establish empirical relations.

5. Acknowledgements

This study was funded by PAI (Pack Ambition International) of the Rhône-Alpes and Auvergne Region, FRANCE.

6. Bibliography

[1] E. Possan, W.A. Thomaz, G.A. Aleandri, E.F. Felix, A.C.P. dos Santos, CO2 uptake potential due to concrete carbonation: A case study, Case Stud. Constr. Mater. 6 (2017) 147–161. doi:10.1016/j.cscm.2017.01.007.

[2] K.L. Scrivener, V.M. John, E.M. Gartner, Eco-efficient cements: Potential economically viable solutions for a low-CO2 cement-based materials industry, Cem. Concr. Res. 114 (2018) 2–26. doi:10.1016/j.cemconres.2018.03.015.

[3] N. Algourdin, B. Sy Hung, Z. Mesticou, A. Si Larbi, Effects of high temperature on mechanical behaviour and physicochemical properties of recycled mortars and its components, Constr. Build. Mater. 248 (2020) 118554. doi:10.1016/j.conbuildmat.2020.118554.

[4] Z. Shui, D. Xuan, W. Chen, R. Yu, R. Zhang, Cementitious characteristics of hydrated cement paste subjected to various dehydration temperatures, Constr. Build. Mater. 23 (2009) 531–537. doi:10.1016/j.conbuildmat.2007.10.016.

[5] M.V.A. Florea, Z. Ning, H.J.H. Brouwers, Activation of liberated concrete fines and their application in mortars, Constr. Build. Mater. 50 (2014) 1–12. doi:10.1016/j.conbuildmat.2013.09.012.

[6] M.C.R. Farage, J. Sercombe, C. Gallé, Rehydration and microstructure of cement paste after heating at temperatures up to 300 °C, Cem. Concr. Res. 33 (2003) 1047–1056. doi:10.1016/S0008-8846(03)00005-X.

[7] Z. Shui, D. Xuan, H. Wan, B. Cao, Rehydration reactivity of recycled mortar from concrete waste experienced to thermal treatment, 22 (2008) 1723–1729. doi:10.1016/j.conbuildmat.2007.05.012.

[8] W. Wang, C. Lu, Y. Li, G. Yuan, Q. Li, Effects of stress and high temperature on the carbonation resistance of fly ash concrete, Constr. Build. Mater. 138 (2017) 486–495. doi:10.1016/j.conbuildmat.2017.02.039.

[9] C. Zhu, Y. Fang, H. Wei, Carbonation-cementation of recycled hardened cement paste powder, Constr. Build. Mater. 192 (2018) 224–232. doi:10.1016/j.conbuildmat.2018.10.113.

[10] H. Justnes, P.A. Dahl, V. Ronin, J.E. Jonasson, L. Elfgren, Microstructure and performance of energetically modified cement (EMC) with high filler content, Cem. Concr. Compos. 29 (2007) 533–541. doi:10.1016/j.cemconcomp.2007.03.004.

[11] J. Skocek, M. Zajac, M. Ben Haha, Carbon Capture and Utilization by mineralization of cement pastes derived from recycled concrete, Sci. Rep. 10 (2020) 1–12. doi:10.1038/s41598-020-62503-z.

[12] T.C.F. Oliveira, B.G.S. Dezen, E. Possan, Use of concrete fine fraction waste as a replacement of Portland cement, J. Clean. Prod. 273 (2020) 123126. doi:10.1016/j.jclepro.2020.123126.

[13] Laboratoire Central des Ponts et Chaussées (France), Recommendations for hardened concretes

under the frost action (in french), 2003.

[14] M. Pigeon, J. Marchand, R. Pleau, Frost resistant concrete, Constr. Build. Mater. 10 (1996) 339–348. doi:10.1016/0950-0618(95)00067-4.

[15] T. Powers, R. Helmuth, Theory of volume changes in hardened Portland cement paste during freezing, in: Portl. Cem. Assoc. Highw. Res. Board, 1953: pp. 286–297.

[16] G. Wardeh, B. Perrin, Relative permeabilities of cement-based materials: Influence of the tortuosity function, J. Build. Phys. 30 (2006) 39–57. doi:10.1177/1744259106064597.

[17] O. Coussy, Poromechanics of freezing materials, J. Mech. Phys. Solids. 53 (2005) 1689–1718. doi:https://doi.org/10.1016/j.jmps.2005.04.001.

[18] G.W. Scherer, Crystallization in pores, Cem. Concr. Res. 29 (1999) 1347–1358. doi:10.1016/S0008-8846(99)00002-2.

[19] R. Zaharieva, F. Buyle-Bodin, E. Wirquin, Frost resistance of recycled aggregate concrete, Cem. Concr. Res. 34 (2004) 1927–1932. doi:10.1016/j.cemconres.2004.02.025.

[20] M. Pigeon, R. Pleau, Durability of Concrete in Cold Climates, E&FN SPON London. (1995) 59–87.

[21] AFGC, Requirements to prevent concrete of freezing-thawing degradation, French Assoc. Civ. Eng. (2018) 1–10.

[22] G. Wardeh, M.A.S. Mohamed, E. Ghorbel, Analysis of concrete internal deterioration due to frost action, J. Build. Phys. 35 (2011) 54–82. doi:10.1177/1744259110370854.

[23] R.M. Salem, E.G. Burdette, N.M. Jackson, Resistance to freezing and thawing of recycled aggregate concrete, ACI Mater. J. (2003) 216–221.

[24] M.R. Geiker, P. Laugesen, On the effect of laboratory conditioning and freeze/thaw exposure on moisture profiles in HPC, Cem. Concr. Res. 31 (2001) 1831–1836. doi:10.1016/S0008-8846(01)00643-3.

[25] W.L. Cao, M.B. Liang, H.Y. Dong, J.W. Zhang, Experimental study on basic mechanical properties of recycled concrete after freeze–thaw cycles, J. Nat. Disasters. 21 (2012) 184–190.

[26] C.Y. Zou, Y.H. Fan, Q. HU, Experimental study on the basic mechanical property of recycled concrete after freeze–thaw, Build. Struct. 40 (2010) 434–438.

[27] M.C. Limbachiya, T. Leelawar, R.K. Dhir, Use of recycled concrete aggregate in high-strength concrete, Mater. Stuctures. 33 (2000) 574–580.

[28] C.S. Rangel, M. Amario, M. Pepe, E. Martinelli, R.D.T. Filho, Durability of structural recycled aggregate concrete subjected to freeze-thaw cycles, Sustain. 12 (2020) 1–21. doi:10.3390/su12166475.

[29] K. Liu, J. Yan, Q. Hu, Y. Sun, C. Zou, Effects of parent concrete and mixing method on the resistance to freezing and thawing of air-entrained recycled aggregate concrete, Constr. Build. Mater. 106 (2016) 264–273. doi:10.1016/j.conbuildmat.2015.12.074.

[30] A. Gokce, S. Nagataki, T. Saeki, M. Hisada, Freezing and thawing resistance of air-entrained concrete incorporating recycled coarse aggregate: The role of air content in demolished concrete, Cem. Concr. Res. 34 (2004) 799–806. doi:10.1016/j.cemconres.2003.09.014.

[31] 196-6 NF EN AFNOR, Methods of testing cement - Part 6: Determination of fineness, (2018).

[32] T. A., The effect of thermal cycling on the durability of concrete made from local materials in the Arabian Gulf countries, Cem. Concr. Researc. 19 (1989) 131–142.

[33] AFNOR, Methods of testing cement - Part 1: Determination of strength, NF EN 196-1. (2016).

[34] P.M.J. Setzer, CIF-Test - Capillary suction , Internal damage and Freeze thaw Test Reference method and alternative methods A and B, 34 (2002) 515–525.

[35] AFNOR, Methods of testing cement - Determination of shrinkage and swelling, NF P15-433. (1994).

[36] AFNOR, Concrete - Testing hardened concrete - Testing porosity and density, NF P 18-459. (2010).

[37] M. Pigeon, Microstructure and freezing-thawing resistance of cements and concretes, PhD thesis, Université de Pierre et Marie Curie, 1984.

[38] M. Chabannet, Internal freeze of cement matrix under mechanical loading, PhD thesis, Institut National des Sciences Appliquées de Lyon, 1994.

[39] V. Baroghel-Bouny, A. Ammouche, H. Hornain, J. Gawsewitch, Microstructural caracterisation of concretes from 25 to 120 MPa, Bull. Des Lab. Des Ponts Chaussees. (2000) 71–86.

[40] J. Skocek, M. Zajac, M. Ben Haha, G. Bolte, Use of carbonated recycled concrete fines as supplementary Cementitious material, 2019.

[41] S. Omary, E. Ghorbel, G. Wardeh, Relationships between recycled concrete aggregates characteristics and recycled aggregates concretes properties, Constr. Build. Mater. 108 (2016) 163–174. doi:10.1016/j.conbuildmat.2016.01.042.

[42] Z.R. Wang, B. Li, H.B. Liu, Y.X. Zhang, X. Qin, Degradation characteristics of graphite tailings cement mortar subjected to freeze–thaw cycles, Constr. Build. Mater. 234 (2020) 117422. doi:10.1016/j.conbuildmat.2019.117422.

[43] N. Tenoutasse, A.M. Marion, Influence of industrial by-products on the porosity of hydrated Portland cement, in: Proceeding 3rd Internatinal Conf. Fly Ash, Silica Fume, Slag Nat. Pozzola, Concr., ACI SP-114, 1989: pp. 33–40.

[44] E.J. Jacobsen, S. Sellevold, Rapid freeze/thaw testing of concrete - Pore structure changes by craking and healing, Concr. under Sev. Cond. Environ. Load. 1 (1995) 114–125.

[45] A. Fabbri, Physics and mechanics of cementitious media submitted to frost action, PhD thesis, Université de Marne-La-Vallée, 2006.

[46] S. Béjaoui, E. Revertegat, J.-P. Bournazel, Mécanismes d Mécanismes de gel des bétons, French Rev. Civ. Eng. 6 (2002) 7–8.

[47] N. Algourdin, Z. Mesticou, A. Si Larbi, Enhancement of recycled concretes properties by accelerated carbonation, Cem. Concr. Compos. 16 (2021). Preprint.

[48] P. Bousquie, Texture and porosity of calcaria rocks (in french), Thèse de doctorat, Université Paris VI et Ecole des Mines de Paris, 1979.

[49] W. Zhang, Y. Pi, W. Kong, Y. Zhang, P. Wu, W. Zeng, F. Yang, Influence of damage degree on the degradation of concrete under freezing-thawing cycles, Constr. Build. Mater. 260 (2020) 119903. doi:10.1016/j.conbuildmat.2020.119903.

[50] O. Helson, Thermo-hydro-mechanical behavior and durability of soil concretes: influence of formulation parameters and exposure conditions., PhD thesis, Université de Cergy-Pontoise, 2017.

[51] J. Xiao, D. Lu, J. Ying, Durability of recycled aggregate concrete: An overview, J. Adv. Concr. Technol. 11 (2013) 347–359. doi:10.3151/jact.11.347.

[52] S.T. Yildirim, C. Meyer, S. Herfellner, Effects of internal curing on the strength, drying shrinkage and freeze–thaw resistance of concrete containing recycled concrete aggregates, Constr. Build. Mater. 91 (2015) 288–296. doi:10.1016/j.conbuildmat.2015.05.045.

[53] Z. Prošek, J. Trejbal, V. Nežerka, V. Goliáš, M. Faltus, P. Tesárek, Recovery of residual anhydrous clinker in finely ground recycled concrete, Resour. Conserv. Recycl. 155 (2020). doi:10.1016/j.resconrec.2019.104640.

[54] C. Girodet, Damage of mortars under thermo-mechanical stress, Phd thesis, Université Claude Bernard, 1996.

[55] AFNOR, Concrete - Freeze test on hardened concrete - Freeze in water - Thaw in water, NF P 18-424. (2008).